Mathematical Modeling and Aerothermal Simulation of a Small-scale Solar Updraft Power Generator

Hadyan Hafizh *, Ahmad Fudholi **‡, M. H. Yazdi ***, Abrar Ridwan****

* Faculty of Mechanical and Manufacturing Engineering Technology, Universiti Teknikal Malaysia Melaka, 76100 Durian Tunggal, Melaka, Malaysia

** Solar Energy Research Institute, Universiti Kebangsaan Malaysia, 43600, Selangor, Malaysia

***Department of Electric Power Generation Stations, Network and Supply Systems, Institute of Engineering and Technology, South Ural State University, 76, Lenin Avenue, Chelyabinsk, 454080, Russian Federation

**** Department of Mechanical Engineering, Universitas Muhammadiyah Riau, 28291 Pekanbaru, Riau, Indonesia

(hadyan@utem.edu.my; a.fudholi@ukm.edu.my, mohammadhossein.yazdi@gmail.com, abrar.ridwan@umri.ac.id)

‡ Corresponding Author; Hadyan Hafizh, Ahmad Fudholi, Universiti Teknikal Malaysia Melaka, 76100 Durian Tunggal, Melaka, Malaysia, Tel: +60 6270 4322,

hadyan@utem.edu.my, a.fudholi@ukm.edu.my

Received: 05.09.2020 Accepted:01.10.2002

Abstract- In this study, an integrated mathematical model is developed to simulate the updraft velocity and temperature of airflow inside a small-scale solar updraft power generator. The model is derived for axisymmetric and inviscid flow conditions where the kinetic energy of the airflow is extracted by using a wind turbine generator. A numerical model based on energy balances at the component level of a small-scale solar updraft power generator is proposed and validated with existing experimental data. The applicability of heat transfer correlations is assessed through computed Rayleigh and Reynolds numbers. All correlations maintain a fast convergence and remain in their range of validity throughout the iteration. Simulation results further reveal that heat losses at the edge of the collector have significant effects and play an important role in both updraft velocity and temperature of airflow. About 3 W/m^2 of heat loss to the edge of the collector was obtained from simulation result. The comparison between simulation and experimental data demonstrates that both results are in good agreement.

Keywords Heat transfer, solar collector, power generator, wind turbine, aerothermal, solar updraft.

1. Introduction

The solar updraft power generator is a renewable energy technology that utilizes solar radiation to create artificial wind for generating electricity [1]. It consists of 3 main components: collector, tower and wind turbine [2]. In the pursuit of increasing total efficiency of the solar updraft power generator, a reliable and simple mathematical model is an essential factor for studying the solar updraft power generator [3,4,5]. The performance of the solar updraft power generator can be predicted by using the developed mathematical model [6,7]. Its efficiency can also be improved by exploiting the developed model through a parametric study [8,9]. This includes examining the effects of solar updraft power generator's geometry such as collector radius, tower diameter and tower height along with ambient temperature conditions [10,11]. Some hybridisation concepts were also introduced such as using the hybrid transpired solar collector that consists of PV panels and a transparent collector [12,13]. An increment of 2% of efficiency from a stand-alone PV system was obtained for a hybrid solar updraft power generator. Furthermore, integration of solar PV and solar collector to

form a hybrid solar updraft power generator was also explored in [14,15].

Developing a highly accurate model is often avoided due to the complex process involved in deriving the mathematical model. The computational fluid dynamic (CFD) simulation can also predict the performance of a solar updraft power generator [31] however, it requires a further step in converting the velocity, pressure and temperature distribution into mechanical power produced by the turbine [16,17]. Despite the recent advances of computing capability in numerical simulations, a simple and traceable mathematical model remains the first choice in studying the energy balance mechanism of a solar updraft power generator.

The ability to reveal and track the complex energy transformation within the solar collector is one of the main purposes for developing a mathematical model. By knowing the mechanism of energy transformation at the solar collector, a parametric study can then be performed to maximise its efficiency. Enhancing efficiency at the collector level and at the tower level will contribute to the overall efficiency of the solar updraft power generator. Therefore, the current work developed a traceable and simple mathematical model of a small-scale solar updraft power generator to provide numerical tools for improving its efficiency.

The present work has objective to develop an integrated mathematical model in assessing the aerothermal characteristic of solar updraft power generator. To comprehensively address the research objective, the framework as illustrated in Fig. 1 is applied.

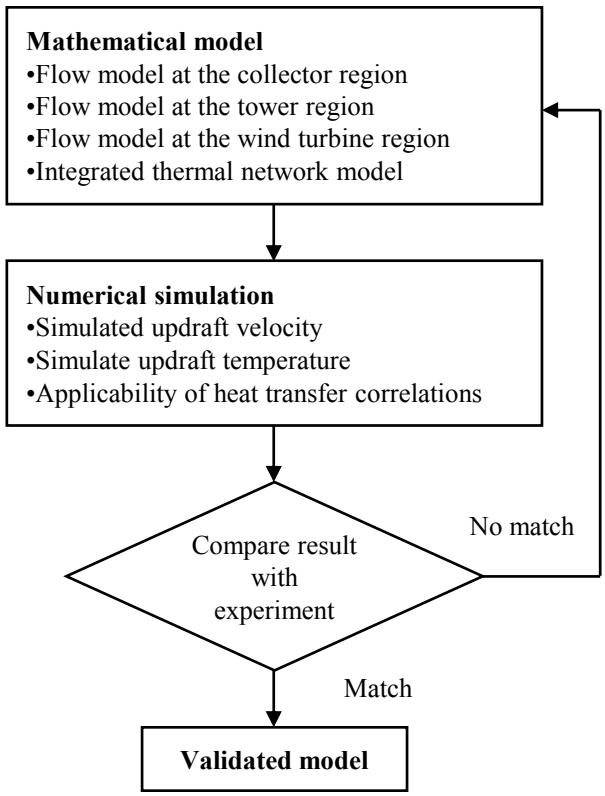

Fig.1. Flowchart of the applied framework.

2. Mathematical Modelling

2.1. Governing equations

The fundamental governing equations of fluid dynamics (such as continuity equation, momentum equation and energy equation) are used as the basic equations for deriving a simple mathematical model. Assumptions employed in the process of forming the mathematical model includes steady-state, axisymmetric and inviscid flows. A state equation is also included in the derivation of the mathematical model to obtain a relationship between temperature, pressure and specific volume of the working fluid. The working fluid is treated as the ideal gas with Boussinesq's hypothesis which deals with the buoyancy force.

The fundamental governing equations are then simplified by using the aforementioned assumptions and the results are presented in Table 1 [18]. The simplified fundamental governing equations along with the ideal gas equation are applied to develop the mathematical models at the solar collector. The momentum and energy equations are utilized to obtain the model of working fluid at the tower region where the relation between pressure drop and harvested mechanical energy is established.

Table 1. Various Input Parameters for Simulation.

Fundamental Equations	Simplified Equations	
Continuity equation	$\frac{1}{r}\frac{\partial}{\partial r} r\rho u_r = 0$	(1)
Momentum equation	$\rho u_r \frac{\partial u_r}{\partial r} + \frac{\partial p}{\partial r} = 0$	(2)
Energy equation	$\rho u_r c_p \frac{\partial T}{\partial r} + \frac{\partial \dot{q}}{\partial r} = 0$	(3)
State equation	$p = \rho RT$	(4)

2.2. Flow Model at the Collector Region

To derive the mathematical model at the collector region, a cross-sectional model of flow inside the collector is examined. A cylindrical coordinate system (r-θ-z) is assigned at the collector region and the flow is axisymmetric in the z-axis, as shown in Fig. 2. In this figure, a schematic drawing of flow passing through a control surface of area *dr* and *dz* is illustrated.

The radial air velocity u_r is flowing in the radial coordinate r with density ρ. The mass flux passes in the normal direction per unit time through the collector area A_{col}. Therefore, the mass flow rate $\dot{m}$ inside the collector can be written as:

$$\dot{m} = \rho u_r A_{col} \tag{5}$$

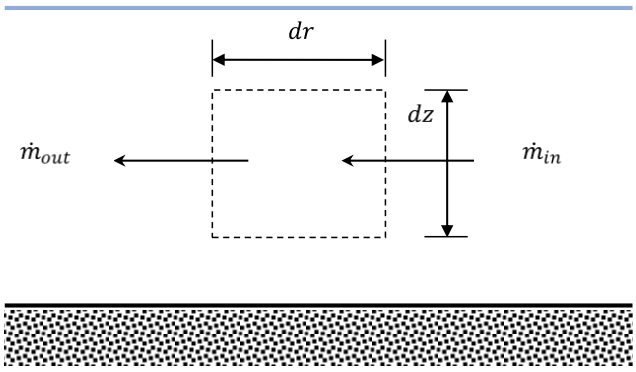

Fig. 2. Schematic drawing for derivation of mass flow rate equation.

To enforce the axisymmetric flow condition, the collector's differential height *dz* must be multiplied with the circumference of the collector's cross-sectional area $2\pi r$. Integration of the collector's differential height from $z = 0$ (ground surface) to $z = h$ (collector height) provides the following expression of the collector area:

$$A_{col} = 2\pi r h_{col} \tag{6}$$

The next step in deriving the mathematical models at the collector region is to obtain an expression of temperature equation. This equation will describe the airflow temperature (T) profile along the radial direction as a function of the collector radius. The simplified fundamental energy equation is employed to develop the temperature equation from a cross-sectional model of airflow, as shown in Fig. 3.

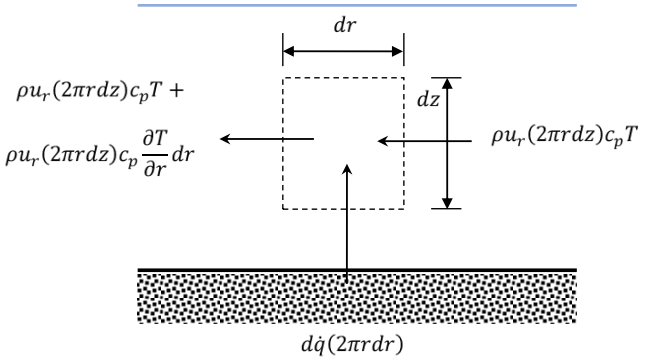

Fig. 3. Schematic drawing for derivation of temperature equation.

In this figure, two heat fluxes are involved in the modelling process: i.e., radiation heat flux and airflow heat flux. Radiation heating is modelled as infinitesimal heat flux $d\dot{q}$ given to the airflow. Thus, the differential airflow will gain energy in the form of heat flux $\rho u_r c_p T$ across the radial direction. The energy balance of this process is written in the form of the power balance equation as:

$$-\rho u_r(2\pi r dz)c_p \frac{\partial T}{\partial r} dr = d\dot{q}(2\pi r dr) \tag{7}$$

Imposing the axisymmetric condition to the temperature equation requires the collector's differential height *dz* to be multiplied by the circumference of the collector's cross-sectional area $2\pi r$. Integration is performed with lower and upper boundaries, respectively, as $z = 0$ and $z = h$. Furthermore, the normal surface for radiation heat flux is assigned as $2\pi r dr$ due to the upward convection process from the ground to the airflow.

Five physical parameters appear in Eq. (7): airflow temperature T, density ρ, radial velocity u_r, specific heat capacity c_p and radiation heat flux $\dot{q}$. The airflow temperature profile can be obtained by further simplifying Eq. (7) where integration and some cancellation terms are performed. The result of integration is given as:

$$T_a(r) = T_{a_\infty} + \frac{d\dot{q}}{\dot{m}c_p}\pi({r_{col}}^2 - r^2) \tag{8}$$

Eq. (8) represents the airflow temperature distribution along the radius of the collector where ambient air temperature T_{a_∞} serves as the initial condition. This equation is also the function of mass flow rate $\dot{m}$ and radiation heat flux $\dot{q}$. The airflow temperature profile extends from the outer radius r_{col} to the variable inner radius of collector r.

2.3. Flow Model at the Tower Region

To derive the mathematical model at the tower region, a cross-sectional model of the flow inside the tower is examined, as shown in Fig. 4. In this figure, the airflow is moving upward in the *z*-axis of the tower. The heated airflow from the collector will rise inside the tower and be released to the atmosphere due to its buoyancy forces. The hot air inside the tower is less dense than the cold air in the atmosphere, thus creating a continuous updraft flow as long as there is a density difference. This density difference is expressed as Boussinesq's fluids which relates to the change of airflow density with the change of airflow temperature. From the boundary layer equation, the change of airflow temperature has a relation with the pressure gradient. Therefore, the updraft velocity inside the tower can be expressed in the form of temperature differences between airflow inside and outside the tower.

The updraft flow inside the tower is moving in the positive z-axis and the gravity acts in the negative z-axis. It is essential to include gravitational force in the mathematical model since it cannot be neglected from the momentum equation. This gravitational force is expressed as $\rho g dz$ in Fig. 4. Since the flow is assumed to be inviscid, the viscous force expression is neglected in Fig. 4. Only inertia and buoyancy forces are included in the modelling process.

Therefore, the net moment flux of airflow inside the tower can be expressed as:

$$\rho u_z \frac{\partial u_z}{\partial z} dz = p - \left(p + \frac{\partial p_z}{\partial z} dz\right) - \rho g dz \quad (9)$$

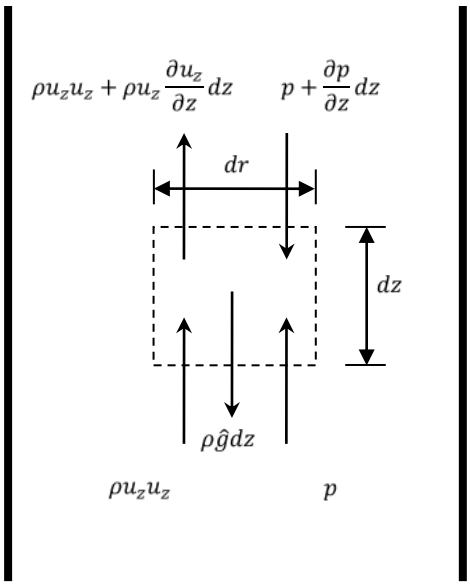

Fig. 4. Schematic drawing for derivation of updraft velocity equation.

The tower inlet in Fig. 4 is also referred to the collector outlet. Thus, Eq. (9) can be viewed as a pressure balance equation at the collector outlet with those at the tower inlet. However, the expression for pressure distribution along the tower height requires further elaboration. The convection process inside the tower is modelled as free convection and by using the Boussinesq's approximation [19] it can be written as follows:

$$\frac{\partial p}{\partial z} = -\rho_{T=T_a} g \quad (10)$$

Eq. (10) portrays the pressure gradient along the tower height. In this equation, the pressure difference can be represented by the density difference at two different values of temperature. By substituting Eq. (10) with Eq. (9) and integrating along the tower height, a solution for updraft velocity u_z can be obtained. The result of the integration process is presented as:

$$u_z = \sqrt{2g \frac{T_a - T_{a\infty}}{T_{a\infty}} h_{tow}} \quad (11)$$

Eq. (11) illustrates the updraft velocity at the tower inlet or collector outlet. Similar expression of the updraft velocity equation is also found in [20,21]. In this equation, the updraft velocity is the function of temperature differences between airflow inside T_a and outside the tower $T_{a\infty}$. The updraft velocity is also a function of the tower height h_{tow} where a higher tower will produce a higher updraft velocity. It is a challenge to construct an ultra-high tower since it is limited by structural capability, although some efforts are being made to analyse the feasibility of building an ultra-high tower for the solar updraft power generator [22]. An alternative strategy to increase the updraft velocity is by enlarging the temperature differences of airflow and ambient air. This can be realised by providing a great amount of heat, not just limited from radiation heating, but also from other sources such as geothermal [23], biomass [24,27], molten salt [28], PCM [29] and water-storage [30].

2.4. Flow Model at the Wind Turbine Region

In this section, the mathematical model of a wind turbine is derived from the fundamental momentum equation and actuator disk theory [25]. The wind turbine produces electrical energy from the conversion of kinetic energy into mechanical energy. Extraction of kinetic energy from the updraft flow slows down the airflow velocity. This process is modelled as a stream-tube (shown in Fig. 5).

In Fig.5, a stream-tube represents two conditions of airflow: affected and non-affected areas. This stream-tube is created by airflow passing through the turbine blades. It creates a boundary portraying both affected and non-affected areas with respect to the mass of air. When the airflow velocity slows down, it is referred to as the affected area. Undisturbed airflow velocity refers to the non-affected area and thus, the velocity remains the same with those flowing in the tower region. The stream tube can be classified into three regions: the collector, rotor and tower region. In this work, a single wind turbine was selected to be installed at the rotor region.

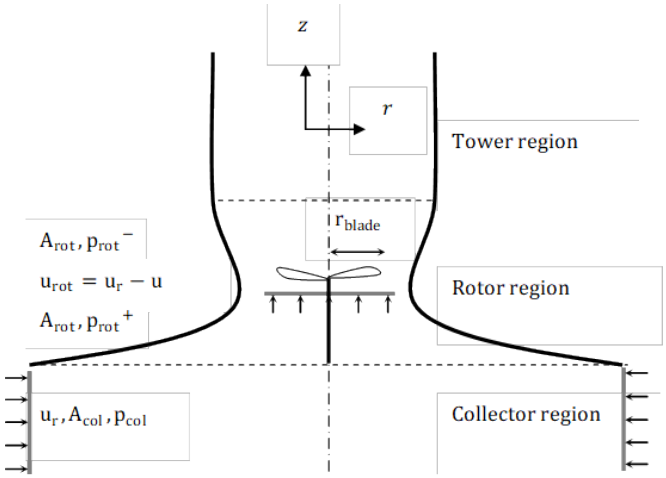

Fig. 5. Schematic drawing for derivation of mechanical power equation.

The amount of airflow velocity from the collector u_r is reduced by a velocity deficit u due to the extraction of its kinetic energy. Thus, the differences between u_r and u become the airflow velocity at the rotor region. Similarly, the pressure at the collector region drops when it passes through the turbine blades. The mechanical power extracted from the airflow is a

function of the velocity deficit. In non-dimensional form, it can be written as inflow coefficient a. This inflow coefficient is obtained by normalising the velocity deficit with airflow velocity from the collector. Mathematically, the mechanical power can be written as a function of the coefficient of power C_P as:

$$P = \frac{\dot{m}^3 C_P}{2\rho^2 \pi^2 {r_{blade}}^4} \tag{12}$$

The coefficient of power C_P has a relationship with the coefficient of thrust $C_{\mathcal{T}}$:

$$C_P = C_{\mathcal{T}}(1-a) \tag{13}$$

The value of $C_{\mathcal{T}}$ is given by the actuator disk theory as:

$$C_{\mathcal{T}} = 4a(1-a) \tag{14}$$

The value of the inflow coefficient depends on the aerodynamic performance of the turbine blades. However, its suitable value can be obtained by performing a numerical parametric study. The result of such a study has found that a value of approximately 2/3 is a suitable choice of inflow coefficient for a solar updraft power generator system [8].

2.5. Integrated Thermal Network Model

To incorporate the velocity and temperature equations at the collector and rotor regions, a thermal network is proposed, as shown in Fig. 6.

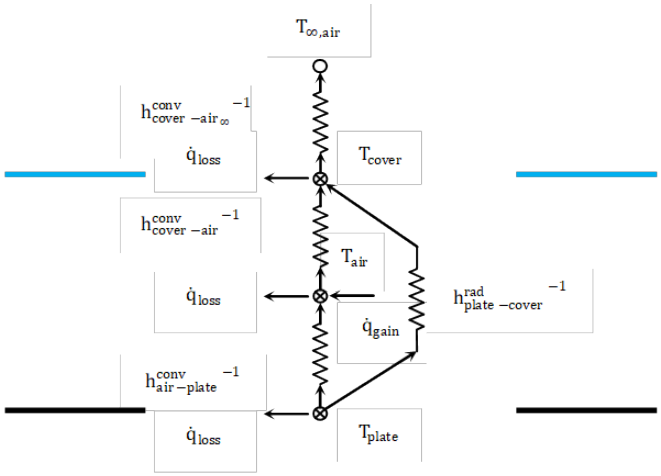

Fig. 6. Thermal network model for small-scale solar updraft power generator.

The thermal network model provides energy balance equation at three different locations: i.e., the plate, airflow and cover. A similar model can also be found in [32]. Two heat transfer modes are selected to model the heat exchange between the plate – airflow, airflow – cover, plate – cover and cover – ambient air. Radiative heat transfer occurs during the heat losses from the plate to the cover while the remaining heat exchanges between the plate, airflow, cover and ambient air are modelled as convective heat transfer. The heat losses from the edge of the collector to ambient air were also considered in the thermal network model. The energy balance equation for each evaluation points are presented in Table 2.

Table 2. Heat balance equation at each evaluation point.

Collector	$-h_{c-a_\infty}^{conv}(T_c - T_{a_\infty}) + h_{a-c}^{conv}(T_a - T_c) + h_{p-c}^{rad}(T_p - T_c) - \dot{q}_{loss} = 0$	(15)
Airflow	$-h_{a-c}^{conv}(T_a - T_c) + h_{p-a}^{conv}(T_p - T_a) + \dot{q}_{gain} - \dot{q}_{loss} = 0$	(16)
Plate	$-h_{p-a}^{conv}(T_p - T_a) - h_{p-c}^{rad}(T_p - T_c) - \dot{q}_{loss} = 0$	(17)

The heat transfer between cover and ambient air is modelled as free convection process and it is characterised by Nusselt number *Nu* [26]. The Nusselt number value depends on the Rayleigh number *Ra* where two correlation functions are used, as presented in Eqs. (18) and (19), and the Prandtl number is denoted as *Pr*.

$$Nu = 0.54Ra(T_a, T_{a_\infty})^{1/4} \quad for \quad 10^4 \le Ra \le 10^7, Pr \ge 0.7 \tag{18}$$

$$Nu = 0.14Ra(T_a, T_{a_\infty})^{1/3} \quad for \quad 10^7 \le Ra \le 10^{11}, all\ Pr \tag{19}$$

A forced convection process is selected to model the convective heat transfer between the plate–airflow and the cover–airflow. The forced convection process is characterised by the Nusselt numbers and correlated via the Reynolds number *Re*. The heat losses from the plate to the airflow is also modelled as a forced convection process. The flow region consists of the laminar and turbulent regions depending on the Reynolds number. Two correlation functions are used in the current work, and they are presented in Eqs. (20) and (21).

$$Nu = \frac{2\sqrt{Re}\sqrt{Pr}}{\sqrt{\pi}(1 + 1.7Pr^{1/4} + 21.36Pr)^{1/6}} \quad Laminar\ flow \quad for \quad Re < 5 \times 10^5, all\ Pr \tag{20}$$

$$Nu = \frac{0.037Re^{0.8}Pr(T_a)}{1 + 2.443Re^{-0.1}[Pr(T_a)^{2/3} - 1]} \quad Turbulent\ flow \quad for \quad 5 \times 10^5 < Re < 10^7, \ and \ 6 \times 10^{-1} < Pr < 2 \times 10^3 \tag{21}$$

Lastly, the heat exchange between the plate and cover is modelled as radiative heat transfer where two infinite parallel surfaces exchange infrared radiation.

2.6. Numerical Simulation

The heat balance equations are then transformed into a matrix equation. They consist of heat flux matrix, temperature matrix and heat transfer coefficients matrix. Each matrix contains unknown parameters, such as the temperature profile along the radius of the collector and updraft velocity. The heat transfer coefficients are also the functions of temperature and updraft velocity. In addition, the heat transfer correlations are in nonlinear forms. Thus, in order to solve the equation, an iterative approach was implemented. The iterative algorithm to solve the heat balance equation is presented in Fig. 7.

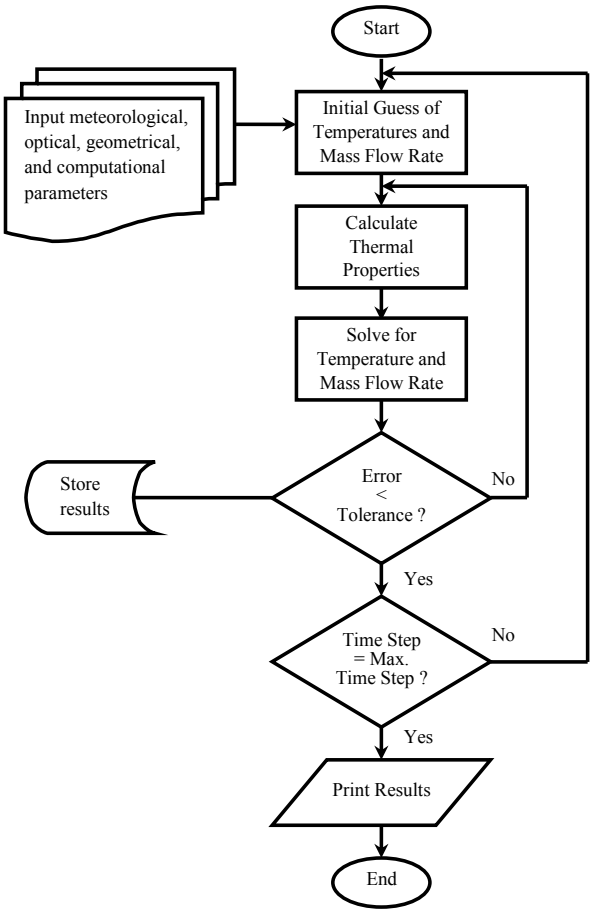

Fig. 7. Flow chart of the developed computer program.

The code was first written in the MATLAB environment and then used to simulate the aero-thermal characteristic of a small-scale solar updraft power generator.

A set of meteorological and optical data must be provided before conducting the simulation. The geometrical data such as the collector radius, tower diameter and height are also required in the simulation process. Examples of meteorological data include ambient air temperature and plate's surface temperature as replacements of solar radiation data. Optical data includes transmissivity, absorptivity and emissivity of plate and cover. A summary of geometrical and optical data used in the simulation is presented in Table 3.

Table 3. Geometrical and optical data for simulation

Parameter	Value
Collector radius	0.5 m
Tower diameter	0.1 m
Cover absorptivity	0.04
Aluminium plate emissivity	0.09

3. Results and Discussion

A numerical simulation to predict the aero-thermal characteristics of a small-scale solar updraft power generator is discussed in this section. The experimental model of the solar updraft power generator used in the current work is shown in Fig. 8. In this figure, a collector, aluminium plate and tower were combined to form a small-scale solar updraft power generator. The collector and the tower are made from poly(methyl methacrylate), also known as acrylic glass. A heat source consisting of an electrical heating element was placed beneath the aluminium plate and surrounded by isolator material to allow heat to only flow in the upwards direction. The heat was then absorbed by the aluminium plate where its temperature was recorded to be used in the numerical simulation.

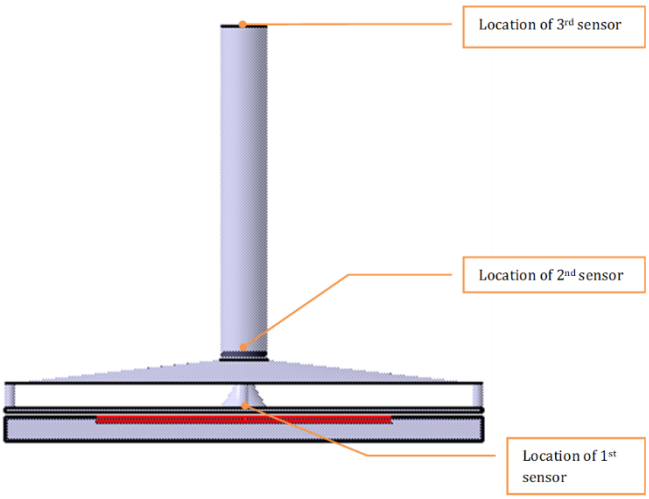

Fig. 8. Schematic diagram of experimental model.

In order to measure the updraft temperature and velocity, two sensors are employed in the experimental work. The first sensor is thermocouple placed on the centre of the aluminium plate to measure the plate's surface temperature. The second sensor is thermo-anemometers installed at the turbine region and the top of the tower. The sensors at the turbine region are used to measure the updraft temperature and velocity of the airflow, while the sensor at the top of the tower is used to measure the velocity and temperature of the exit updraft flow. The measurement was performed for 60 minutes and the data

were sampled every 1 minute. The collected data were then compared with those from the simulation results.

3.1. Simulated Updraft Temperature and Velocity

The updraft temperature and velocity are simulated by solving Eqs. 15–17 using the developed computer program. Simulations were carried out for time step 1 to 60 minutes. Since the updraft temperature and velocity of the airflow are influenced by the heat losses to the environment, the simulations were performed for five different values of heat loss, starting from 1 W/m^2 to 5 W/m^2.

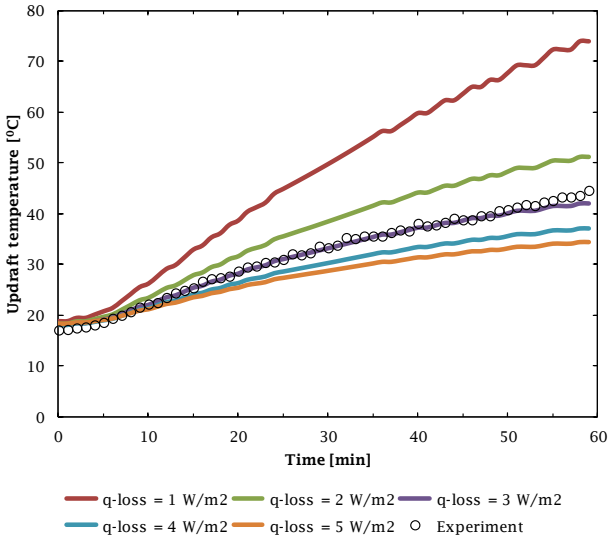

Fig. 9a. Simulated and experimental updraft temperature.

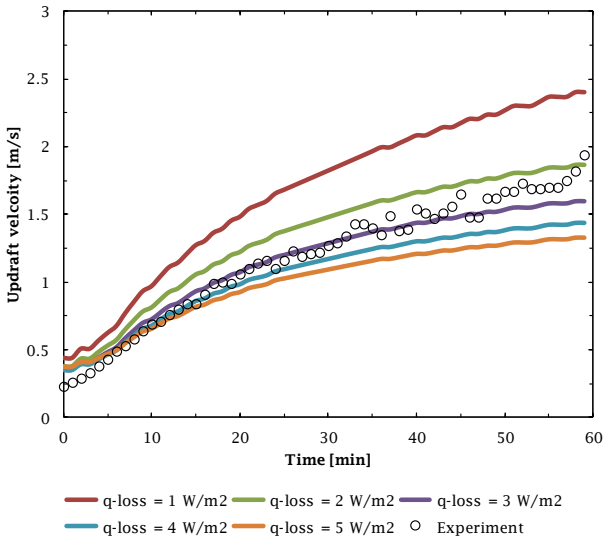

Fig. 9b. Simulated and experimental updraft velocity

Furthermore, the heat transfer correlation representing heat losses to the environment are not generally available in the literature. Hence, as assumed, the magnitude of heat loss to the environment holds a constant value throughout time. Fig. 9a shows the simulated updraft temperature for five different cases of heat loss. It can be seen in this figure that the small heat loss value produces an overestimate result of updraft temperature, in particular for 1 W/m^2 and 2 W/m^2. On the other hand, a large heat loss value yields an underestimate of updraft temperature numbers. An optimum heat loss value was found to be approximately 3 W/m^2.

In the case of simulated updraft velocity, a similar situation was observed where an optimum value for heat loss is around 3 W/m^2. The simulated and experimental results of updraft velocity are presented in Fig. 9b. In this figure, the updraft velocity was simulated for five different heat loss values. Overestimation of updraft velocity was also observed for the series of low heat loss values. The series of high heat loss values yielded an underestimate of updraft velocity numbers. A consistent result was obtained for both the updraft temperature and velocity. Therefore, the developed mathematical model can predict the aero-thermal characteristic of airflow inside a small-scale solar updraft power generator.

3.2. Applicability of Heat Transfer Correlations

In order to examine the validity of heat transfer correlations, a numerical parametric study was performed. The purpose of this study is to closely examine the applicability of heat transfer correlations used in the numerical simulation. This study is essential since all heat transfer correlations employed in the current work are based on empirical relations that have their range of validity. Two non-dimensional numbers characterise the employed heat transfer correlations: the Rayleigh number and the Reynolds number. The study was conducted by assessing these two non-dimensional numbers throughout the simulation process. A numerical simulation to calculate the updraft temperature and velocity was performed for time steps 1 to 60 minutes. For each time step, the Rayleigh and the Reynolds numbers were assessed, and the results are presented in Figs. 10.

Fig. 10a shows the simulated Rayleigh numbers where their values influence the Nusselt number. The Nusselt number correlation, as in Eqs. 18 and 19, was used to characterise the heat transfer between the cover and ambient air. The Nusselt number was correlated for two regions of the Rayleigh numbers where Equation 18 was applied for $10^4 \leq Ra \leq 10^7$ and Equation 19 was applied for $10^7 \leq Ra \leq 10^{11}$.

The simulated Rayleigh numbers in Fig. 10a indicate that they were computed in their valid range, although some fluctuations were observed in the beginning of iteration. It was also observed that the computed Rayleigh numbers switched during the iteration process before attaining a convergence value. The switching Rayleigh numbers illustrate that a lower range of Rayleigh numbers was used in the beginning of

simulation and after approximately 5 minutes, a higher range of Rayleigh numbers was employed in the simulation process.

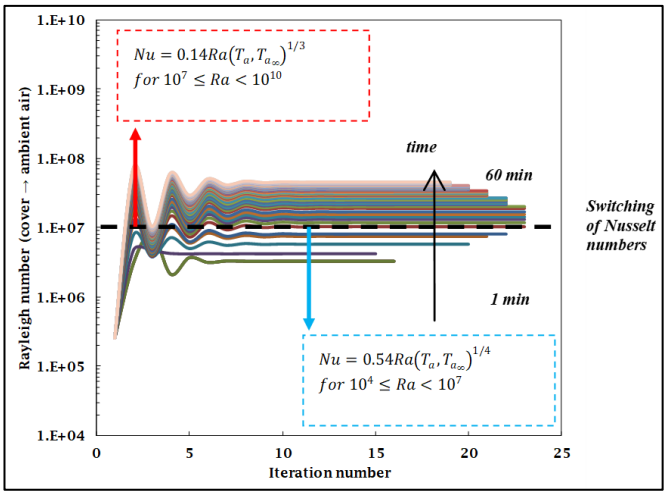

Fig. 10a. Computed Rayleigh number

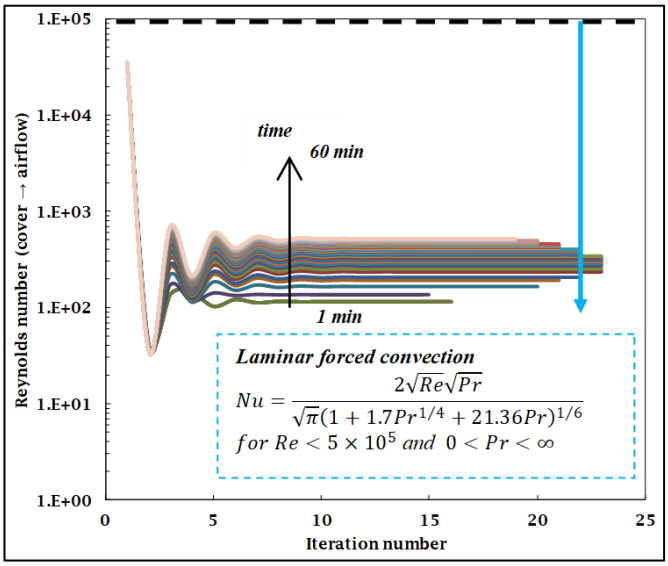

Fig. 10b. Computed Reynolds number

Fig. 10b presents the computed Reynolds number during the simulation process. The associated Nusselt number in this figure was applied to characterise the heat transfer process between the plate – airflow and cover – airflow. Two heat transfer correlations were prepared for the simulation process (Eqs. 20 and 21). The two correlation functions were used for laminar and turbulent flow conditions. Based on the computed Reynolds number, it was found that the flow stays in the laminar condition throughout the simulation time. Nevertheless, the computed Reynolds number remained in its range of validity.

4. Conclusion

In this study, a mathematical model of a small-scale solar updraft power generator was proposed where the energy balance equations from the thermal network model were solved using the developed computer program. The simulation results were validated by comparing the simulated updraft temperature and velocity with those from the experiment. It was demonstrated that both results are in good agreement with the inclusion of heat losses model. Simulation results demonstrated how the heat losses at the edge of the collector play an important role in the accuracy of calculated results. The suggested value of heat loss for a small-scale solar updraft power generator model is approximately 3 W/m^2.

The applicability of heat transfer correlations employed in the simulation was discussed and assessed through computed Rayleigh and Reynolds numbers. It was found that both Rayleigh and Reynolds numbers were in the valid range throughout the iteration process. The potential future application of the proposed method would be a tool that manages to evaluate the amount of generated power by a solar updraft power generator. It can be concluded that the developed model has the potential to serve as a numerical tool in helping researchers predict the aerothermal characteristics of a solar updraft power generator system.

References

[1] M. Aurélio dos Santos Bernardes, T. W. Von Backström, and D. G. Kröger "Analysis of some available heat transfer coefficients applicable to solar chimney power plant collectors," Sol. Energy, vol. 83, no. 2, pp. 264–275, 2009.

[2] F. Cao, H. Li, Q. Ma, and L. Zhao, "Design and simulation of a geothermal-solar combined chimney power plant," Energy Convers. Manag., vol. 84, pp. 186–195, 2014.

[3] P. J. Cottam, P. Duffour, P. Lindstrand, and P. Fromme, "Solar chimney power plants – Dimension matching for optimum performance," Energy Convers. Manag., vol. 194, no. April, pp. 112–123, 2019.

[4] E. Cuce, H. Sen, and P. M. Cuce, "Numerical performance modelling of solar chimney power plants: Influence of chimney height for a pilot plant in Manzanares, Spain," Sustain. Energy Technol. Assessments, vol. 39, no. January, p. 100704, 2020.

[5] M. A. dos, A. Voß, and G. Weinrebe, "Thermal and technical analyses of solar chimneys," Sol. Energy, vol. 75, no. 6, pp. 511–524, 2003.

[6] A. Habibollahzade, E. Houshfar, M. Ashjaee, A. Behzadi, E. Gholamian, and H. Mehdizadeh, "Enhanced power generation through integrated renewable energy plants: Solar chimney and waste-to-energy," Energy Convers. Manag., vol. 166, pp. 48–63, 2018.

[7] H. Hafizh, R. Hamsan, A. A. A. Zamri, M. F. M. Keprawi, and H. Shirato, "Solar updraft power generator with radial and curved vanes," in AIP Conference Proceedings, 2018, vol. 1930.

[8] H. Hafizh and H. Shirato, "Aerothermal simulation and power potential of a solar updraft power plant," vol. 61A,

pp. 388–399, 2015.

[9] A. Hassan, M. Ali, and A. Waqas, "Numerical investigation on performance of solar chimney power plant by varying collector slope and chimney diverging angle," Energy, vol. 142, pp. 411–425, 2018.

[10] A. B. Kasaeian, E. Heidari, and S. N. Vatan, "Experimental investigation of climatic effects on the efficiency of a solar chimney pilot power plant," Renew. Sustain. Energy Rev., vol. 15, no. 9, pp. 5202–5206, 2011.

[11] W. B. Krätzig, "An integrated computer model of a solar updraft power plant," Adv. Eng. Softw., 2013.

[12] D. Eryener and H. Kuscu, "Hybrid transpired solar collector updraft tower," Sol. Energy, vol. 159, no. November 2017, pp. 561–571, 2018.

[13] D. Eryener, J. Hollick, and H. Kuscu, "Thermal performance of a transpired solar collector updraft tower," Energy Convers. Manag., vol. 142, pp. 286–295, 2017.

[14] S. Kiwan, M. Al-Nimr, and I. Salim, "A hybrid solar chimney/photovoltaic thermal system for direct electric power production and water distillation," Sustain. Energy Technol. Assessments, vol. 38, no. November 2019, p. 100680, 2020.

[15] A. Pratap Singh, A. Kumar, Akshayveer, and O. P. Singh, "Performance enhancement strategies of a hybrid solar chimney power plant integrated with photovoltaic panel," Energy Convers. Manag., vol. 218, no. March, p. 113020, 2020.

[16] T. Ming, W. Liu, and G. Xu, "Analytical and numerical investigation of the solar chimney power plant systems," Int. J. Energy Res., vol. 30, no. 11, pp. 861–873, 2006.

[17] H. Pastohr, O. Kornadt, and K. Gürlebeck, "Numerical and analytical calculations of the temperature and flow field in the upwind power plant," Int. J. Energy Res., vol. 28, no. 6, pp. 495–510, 2004.

[18] J.D. Anderson, Fundamentals of Aerodynamics 6th ed, McGraw-Hill, 2017, pp. 197-200.

[19] C. O. Okoye and U. Atikol, "A parametric study on the feasibility of solar chimney power plants in North Cyprus conditions," Energy Convers. Manag., vol. 80, pp. 178–187, 2014.

[20] M. R. Ahmed and S. K. Patel, "Computational and experimental studies on solar chimney power plants for power generation in Pacific Island countries," Energy Convers. Manag., vol. 149, pp. 61–78, 2017.

[21] M. A. Aurybi, S. I. Gilani, H. H. Al-Kayiem, and A. A. Ismaeel, "Mathematical evaluation of solar chimney power plant collector, integrated with external heat source for non-interrupted power generation," Sustain. Energy Technol. Assessments, vol. 30, no. September 2017, pp. 59–67, 2018.

[22] F. Lupi, C. Borri, R. Harte, W. B. Krätzig, and H. J. Niemann, "Facing technological challenges of Solar Updraft Power Plants," J. Sound Vib., 2015.

[23] F. Cao, H. Li, Q. Ma, and L. Zhao, "Design and simulation of a geothermal-solar combined chimney power plant," Energy Convers. Manag., vol. 84, pp. 186–195, 2014.

[24] A. Habibollahzade, E. Houshfar, M. Ashjaee, A. Behzadi, E. Gholamian, and H. Mehdizadeh, "Enhanced power generation through integrated renewable energy plants: Solar chimney and waste-to-energy," Energy Convers. Manag., vol. 166, no. April, pp. 48–63, 2018.

[25] Y. Liu and S. Yoshida, "An extension of the Generalized Actuator Disc Theory for aerodynamic analysis of the diffuser-augmented wind turbines," Energy, vol. 93, pp. 1852–1859, 2015.

[26] M. Aurélio dos Santos Bernardes, T. W. Von Backström, and D. G. Kröger, "Analysis of some available heat transfer coefficients applicable to solar chimney power plant collectors," Sol. Energy, vol. 83, no. 2, pp. 264–275, 2009.

[27] X. Zhou and Y. Xu, "Daily dynamic performance of a solar chimney power plant integrated by waste heat recovery," IET Renew. Power Gener., vol. 14, no. 2, pp. 270–274, 2020.

[28] S. Saengsaen, C. Thongkroy, W. Wechsatol, and C. Chantharasenawong, "Design an efficiency assessment of solar thermal updraft tower with molten salt as heat storage," 1st IEEE Student Conf. Electr. Mach. Syst. SCEMS 2018, no. 2, pp. 3–7, 2019.

[29] J. C. F. Dordelly, M. El Mankibi, and M. Coillot, "Numerical and experimental investigations of a PCM integrated solar chimney," 2018 4th Int. Conf. Renew. Energies Dev. Countries, REDEC 2018, 2018.

[30] S. Larbi, A. Bouhdjar, K. Meliani, A. Taghourt, and H. Semai, "Solar chimney power plant with heat storage system performance analysis in South Region of Algeria," Proc. 2015 IEEE Int. Renew. Sustain. Energy Conf. IRSEC 2015, 2016.

[31] E. Gholamalizadeh and J. D. Chung, "A Parametric study of a pilot solar chimney power plant using cfd," IEEE Access, vol. 6, pp. 63366–63374, 2018.

[32] E. F. Abbas, T. A. Tahseen, and S. Y. Hassan, "Experimental investigation for a laboratory solar chimney; a practical study in Iraq," Int. J. Renew. Energy Res., vol. 10, no. 2, pp. 1054–1059, 2020.